EMC Characterization of SMPS Devices: Circuit and Radiated Emissions Model

Giulio Antonini, Saverio Cristina, *Senior Member, IEEE,* and Antonio Orlandi, *Member, IEEE*

***Abstract*—Since the efficiency of switched mode power supplies (SMPS) is much higher than that of linear power supplies, this type of supply has gained favor among designers and manufacturers. Switching frequencies extend from tens to hundreds of kilohertz with the result that radiation from circuits carrying switched current is becoming more of a problem. This paper addresses the modeling of the converter section of an SMPS in order to calculate the current distribution and the radiated electromagnetic field. The inhomogeneities in the circuit are treated by equivalent electrical parameters and a technique is introduced to take into account the fictitious effects on radiation due to the electrostatic terms in the dipole equations. The global approach is validated by comparison of the computed results with those measured for a simple and clearly arranged SMPS experimental setup.**

I. Introduction

SWITCHED mode power supplies (SMPS) have now become one of the more popular types of supply. Their use ranges from the feeding of integrated electronic devices to the feeding of power drive systems. According to the definitions given in the new IEC Draft 22G-WG4-11 [1], an SMPS consists of two parts: the so-called converter section and the control section. The former is composed of the switching elements, the auxiliary devices, and the conductors to the load. The switching elements are usually semiconductor devices with switching frequency extending from tens to hundreds of kilohertz. During turn-on and turn-off operations they give rise to very fast voltage and current transients that are sources of conducted and radiated electromagnetic interferences (EMI). Although conducted emissions from the converter section of an SMPS are well covered in the literature, e.g., [2]–[4], their radiated emissions are not. Both the control and the converter sections are sources of radiated emissions. The digital circuits of the control section radiate in the RF range and do not have enough energy to be a serious hazard for the correct operation of the converter section. However, knowledge of the converter sections radiated near-field is extremely important for a correct EMC design of the device: this electromagnetic (EM) radiation has enough energy to affect the operations of the control section, possibly causing malfunctions. This paper addresses the EMC modeling of an SMPS to evaluate current distribution on the converter section and to predict the near EM field radiated.

Manuscript received May 10, 1995; revised February 22, 1996.

G. Antonini and S. Cristina are with the Department of Electrical Engineering, University of Rome "La Sapienza," 00184 Rome, Italy.

A. Orlandi is with the Department of Electrical Engineering, University of L'Aquila, 67040 L'Aquila, Italy.

Publisher Item Identifier S 0018-9375(96)06300-4.

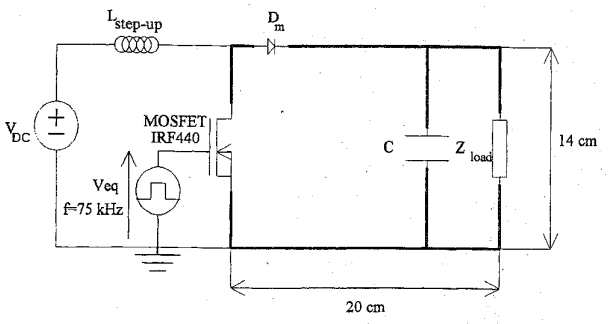

Fig. 1. Schematic of the SMPS.

Following the typical topology of an SMPS, a simple and clearly arranged circuit configuration has been chosen for the simulations; this has been built up for measurement and validation of the numerical results. The schematic of the considered SMPS is shown in Fig. 1, where the control section is simulated by an equivalent square wave pulse generator V_{eq} supplying the gate of the switching element, a MOSFET. V_{DC} is the dc power supply, D_m is the free wheeling diode, $L_{step\text{-}up}$ is an auxiliary inductance which allows the voltage at the load to be raised, and Z_{load} is a generic passive load. The conductors at the right-hand side of the MOSFET are printed traces over an epoxy substrate ($\varepsilon_r = 4.7$). The next section of the paper deals with the circuit model and the per unit length (p.u.l.) electrical parameter estimation required to calculate the current distribution along the traces. Section III is devoted to the introduction of a near-field radiation model in which the dipole equations are adequately modified to treat the fictitious effects of the electrostatic terms [5], [6]. The numerical results obtained by the developed prediction models are presented in Section IV; they are also compared with the measurements performed by means of a test setup described in the same section. The conclusions are given in Section V.

II. Circuit Model of the Converter Section

The highest switching frequencies of an SMPS rarely exceed 200 kHz so it may be expected that there is a band limited spectrum around $f_{max} = 10$ MHz ($\lambda_{min} = 30$ m) of the harmonic components of the current in the converter section. Given the geometrical dimensions of the circuit illustrated in Fig. 1, a circuit approach can be used to analyze the current distribution on the printed traces. The traces are divided into two pairs: horizontal and vertical. Each pair consists of two parallel strips on the same side of the board [see Fig. 2(a)], at the interface between media with different

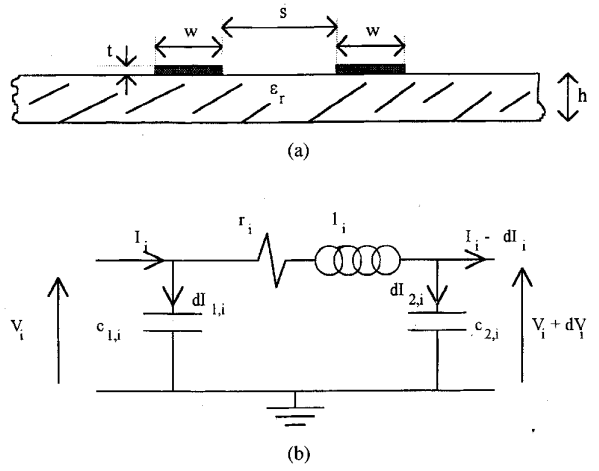

Fig. 2. (a) Cross section of the traces. (b) Elementary lumped Pi section.

dielectric constants. Each pair is considered as a transmission line (TL) and divided into an elementary lumped Pi section, as shown in Fig. 2(b), where r, l, and c are respectively the p.u.l. resistance, inductance and capacitance, evaluated in the following manner:

A. Evaluation of the p.u.l. Resistance

The total resistance r is frequency dependent but the dimensions of the traces are such that even at the highest considered frequency the current can be considered uniformly distributed over the whole cross section. Furthermore, the high impedance of the load permits such a frequency variation of r to be neglected

$$r = r_{\mathrm{DC}} = (\sigma w t)^{-1} \quad [\Omega/\mathrm{m}] \tag{1}$$

where σ is the conductivity of the traces.

B. Evaluation of the p.u.l. Inductance and Capacitance

Owing to the coplanar configuration of Fig. 2(a), the exact evaluation of l and c is difficult, not least because of the presence of an inhomogeneous medium. An effective relative dielectric constant ε_r' is therefore introduced: this is the constant of a fictitious dielectric material such that if the original pair of traces were immersed in a homogeneous material having this constant, the TL would have velocity of propagation

$$v = (\varepsilon_0 \varepsilon_r' \mu_0)^{-1/2} \quad [\mathrm{m/s}]. \tag{2}$$

When $w \gg t$ the following expression for ε_r' can be used [7]

$$\varepsilon_r' = \frac{\varepsilon_r + 1}{2}\left\{\tanh\left[0.775 \ln\left(\frac{h}{w}\right) + 1.75\right] + \frac{kw}{h}[0.04 - 0.7k + (10^{-2} - \varepsilon_r 10^{-3})(0.25 + k)]\right\} \tag{3}$$

where $k = s/(s + 2w)$. For coplanar strips Z_c is given in [8]

$$Z_c = 377 K(k)/(\varepsilon_r')^{1/2} K(k') \quad [\Omega] \tag{4}$$

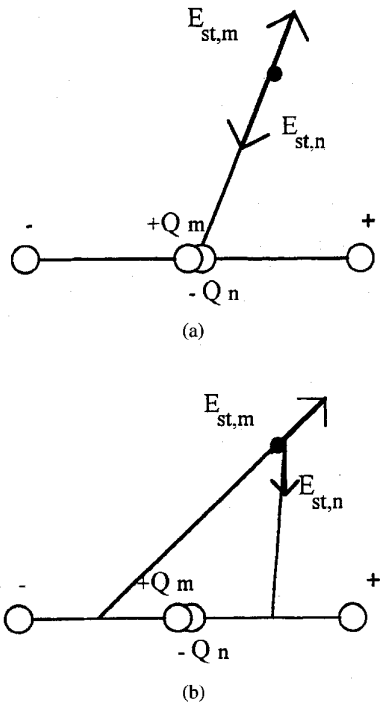

Fig. 3. Effect of the electrostatic term in dipole equations: (a) physical situation and (b) numerical situation.

in which $K(k)$ is the complete elliptic integral of the first kind

$$K(k) = \int_0^1 \frac{dt}{[(1 - t^2)(1 - k^2 t^2)]^{1/2}} \tag{5a}$$

k is the modulus and k' is the complementary modulus defined as

$$k' = (1 - k^2)^{1/2}. \tag{5b}$$

The numerical evaluation of the ratio $K(k)/K(k')$ in (4) is straightforward and accurate; simplex expressions for this ratio are given in Appendix A. The introduction of ε_r' permits the use of the well-known expressions of the TL theory to evaluate the external inductance l_e and c

$$l_e = Z_c/v \quad [\mathrm{H/m}] \tag{6a}$$

$$c = 1/vZc \quad [\mathrm{F/m}]. \tag{6b}$$

For the SMPS the internal inductance is ignored because it is negligible compared with the external one. It should be noted that the electrical parameters in Fig. 2(b) $l = l_e, r = r_{\mathrm{DC}}$ and c represent the two parallel traces and their mutual couplings. As with all the TL models, this one is unable to treat the common mode currents arising from geometrical or electrical circuit asymmetry or stray capacitances toward metallic structures such as heatsinks or EM screens. This fact fixes an upper limit to the frequency range for which the present approach is valid. However, as shown in Section IV, this limit is well above the highest significant harmonic component of the SMPS current.

TABLE I
GEOMETRICAL CHARACTERISTICS OF THE SMPS

	Horizontal Traces	Vertical Traces
l [mm]	200	140
s [mm]	140	200
w [mm]	5	5
t [mm]	0.1	0.1
h [mm]	1.57	1.57

TABLE II
ELECTRICAL PARAMETERS OF THE CIRCUITS

	Horizontal Traces	Vertical Traces
σ [S/m]	$59.7 \cdot 10^6$	$59.7 \cdot 10^6$
ε_r	4.7	4.7
ε'_r	2.74	2.74
v [m/s]	$1.81 \cdot 10^8$	$1.81\ 10^8$
Z_c [Ω]	619.3	648.7
r [Ω /m]	$33.5 \cdot 10^{-3}$	$33.5 \cdot 10^{-3}$
l [μH/m]	3.42	3.58
c [pF/m]	8.92	8.51

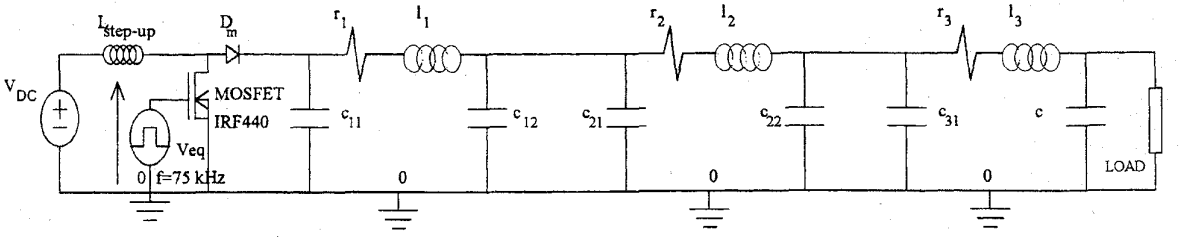

Fig. 4. Complete PSpice circuit adopted for simulations.

The circuit simulator PSpice [9] has been used to calculate the current distribution.

III. NEAR-FIELD RADIATION MODEL

The current flowing in the printed traces of the converter section of the SMPS is considered to be the source of the device's radiated EM field. Because of the width and thickness of the traces and the harmonic content of the current, the cross-sectional variation of the current can be neglected, thus permitting the use of the well known Hertzian (or electric) dipole model of radiation. In frequency domain the dipole equations are [10]

$$E_\vartheta = \frac{I(\omega)\,dl}{4\pi}\sin\vartheta\left[\frac{j\omega\mu_0}{r} + \frac{1}{j\omega\varepsilon_0 r^3} + \frac{\eta_0}{r^2}\right]e^{-jkr} \quad (7a)$$

$$E_r = \frac{I(\omega)\,dl}{4\pi}\cos\vartheta\left[\frac{2}{j\omega\varepsilon_0 r^3} + \frac{2\eta_0}{r^2}\right]e^{-jkr} \quad (7b)$$

$$H_\phi = \frac{I(\omega)\,dl}{4\pi}\sin\vartheta\left[\frac{jk}{r} + \frac{1}{r^2}\right]e^{-jkr} \quad (7c)$$

where $I(\omega)$ is the phasor of the current assumed constant along the length dl of the dipole, r is the distance from the observation point P to the center of the dipole, η_0 is the free-space impedance, k is now the propagation constant and θ the azimuth angle. The radiating traces are considered to be made up of a number of dipoles connected to one another; the total radiated field is the sum of all contributions from each constituent dipole element [5], [6]. In the near-field region the term $1/r^3$ in (7a) and (7b) is predominant. The electric field is proportional to the integral of the current $I(\omega)/j\omega$, that is to say proportional to the equal and opposite sinusoidal time-varying charges Q that, by continuity, must exist on the two ends of the dipole. If more dipoles are connected in series and carry different currents, the equivalent net charge $Q_{m,n}$ at the junction between the mth and nth dipole is given by the requirement of continuity

$$Q_{m,n} = Q_m - Q_n = I_m(\omega)/j\omega - I_n(\omega)/j\omega. \quad (8)$$

If $I_m(\omega) = I_n(\omega)$ then $Q_{m,n} = 0$ and its contribution to the total radiated field from the two dipoles must vanish.

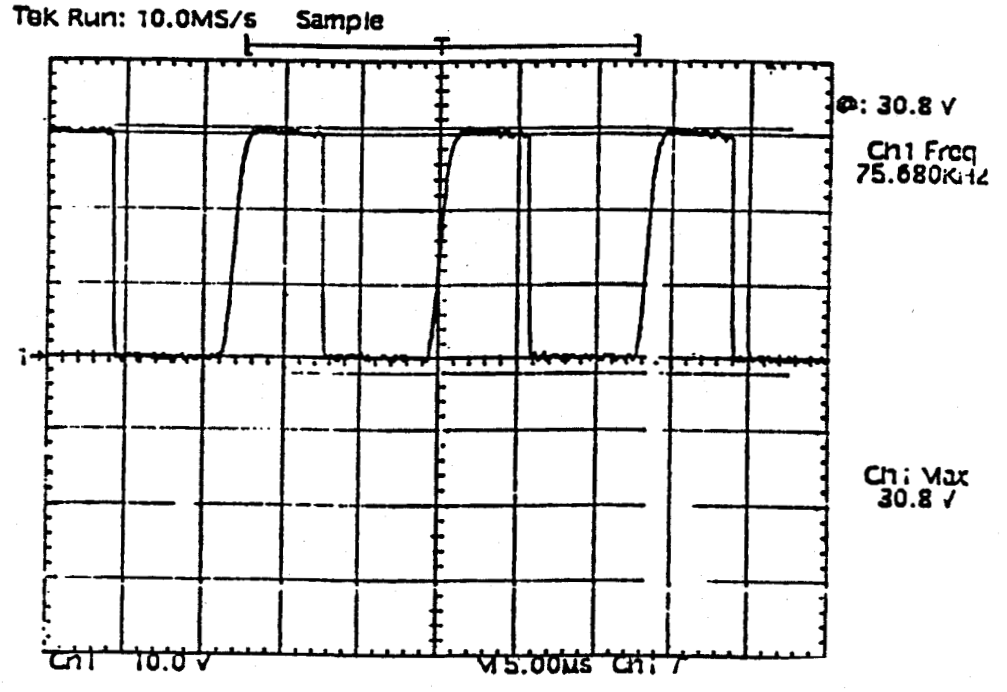

(a)

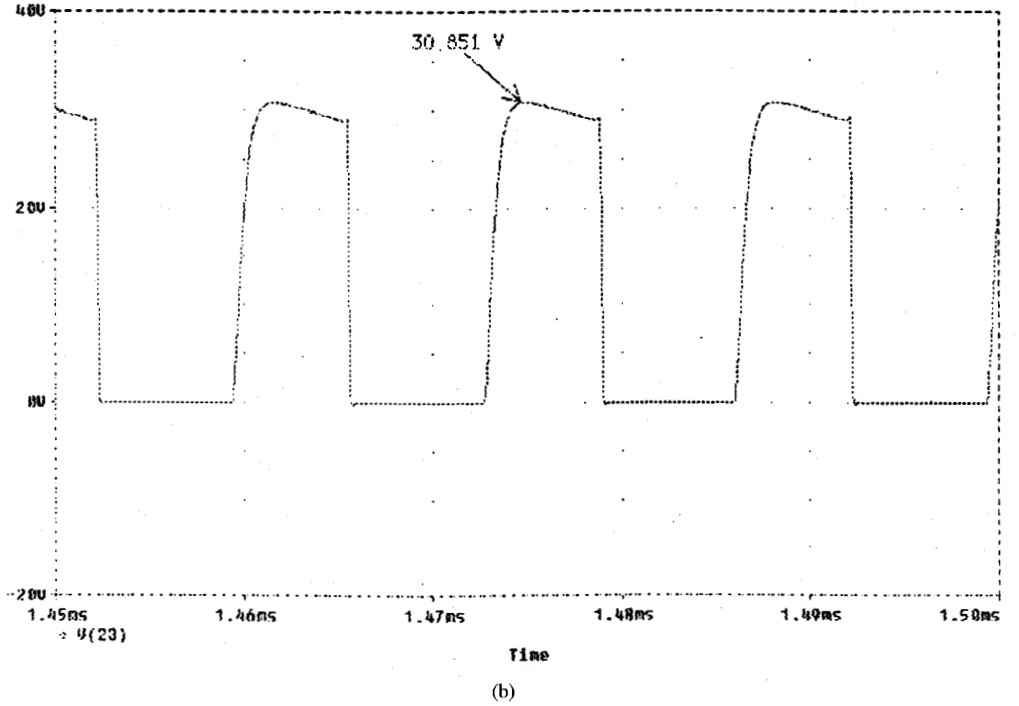

(b)

Fig. 5. Load voltage: (a) measured and (b) computed.

This case is depicted in Fig. 3(a) $\boldsymbol{E}_{st,m}$ and $\boldsymbol{E}_{st,n}$ are due to Q_m and Q_n at the junction. They are equal and opposite, and because the two charges theoretically overlap, they point in the same direction so their vector sum must be zero, as physically expected. The next part of this section is devoted to showing how equations (7) are unable to handle such requirements without adequate correction.

The EM field at the observation point P is evaluated by means of (7) considering the distance from P to the dipole center. This means that in the case of the dipoles m and n mentioned above, $\boldsymbol{E}_{st,m}$ and $\boldsymbol{E}_{st,n}$ do not lie in the same direction and their sum is not zero [see Fig. 3(b)]. This gives rise to a fictitious electric field component that results in the low frequency near-fields being overestimated. When

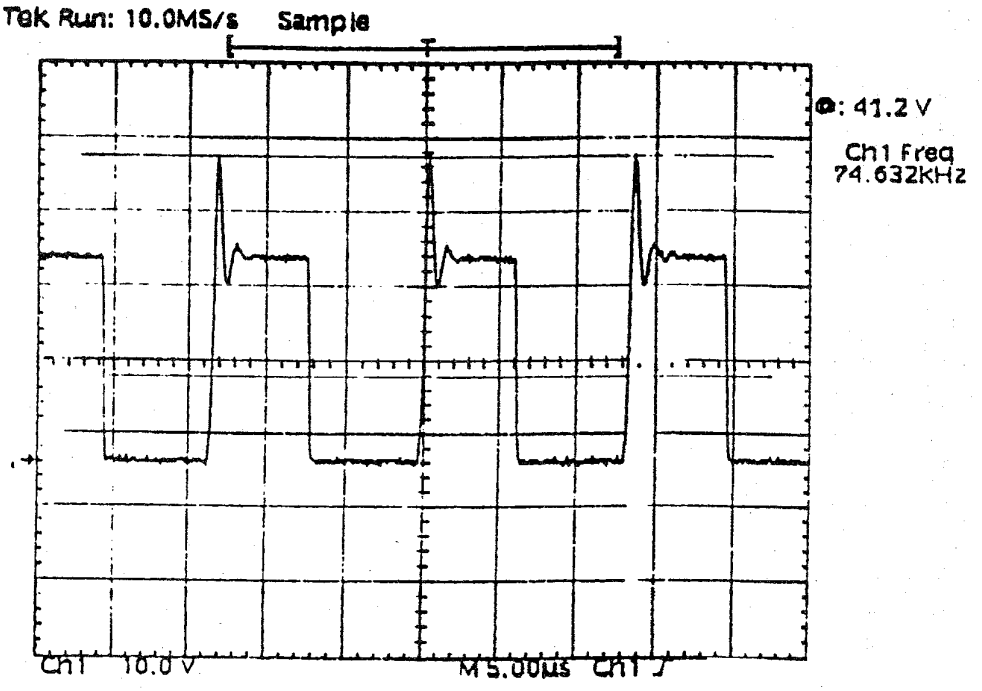

(a)

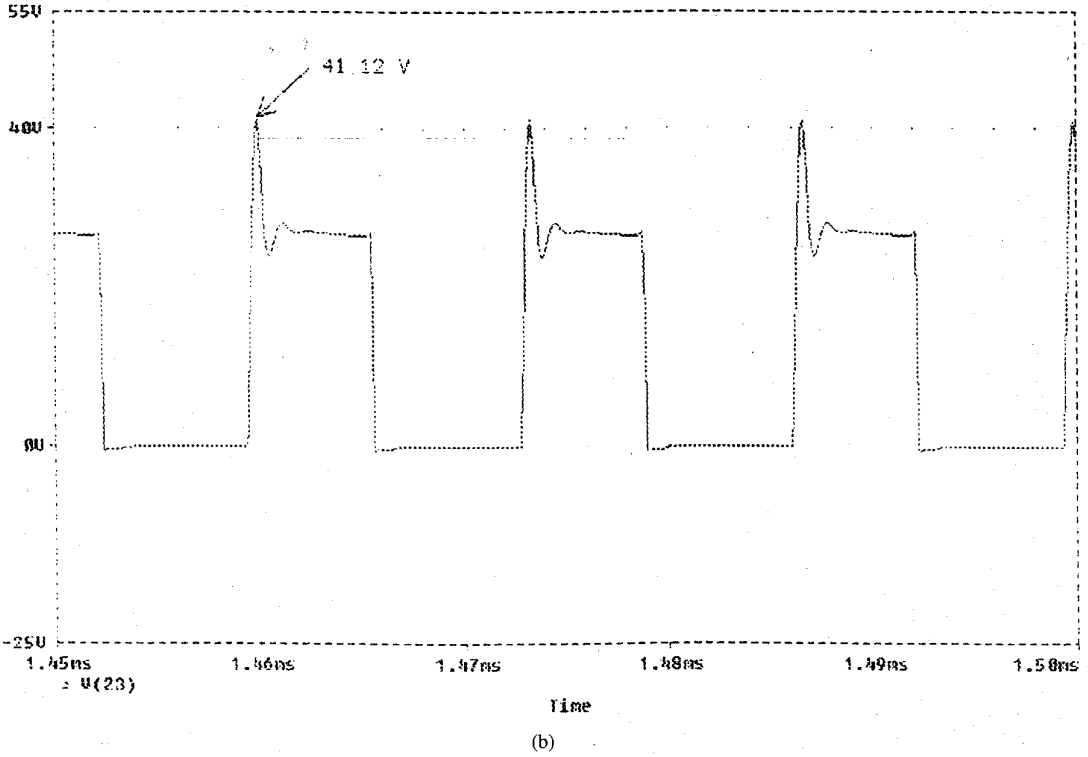

(b)

Fig. 6. —Load voltage: (a) measured and (b) computed.

all dipoles carry the same current (as with electrically short structures), one solution to the problem of such an unnaturally large near-zone term due to consideration of the charges at the dipole centers is to omit from the calculation the electrostatic term in (7), except in the case of the outermost dipoles in open structures or where an accumulation of charges exists, for example, at the leads of a capacitor. For closed structures, the electrostatic term is omitted for all dipoles. If dipoles carry different currents the $1/r^3$ term in (7) is always omitted but the contribution of the net charge $Q_{m,n}$ at each junction is

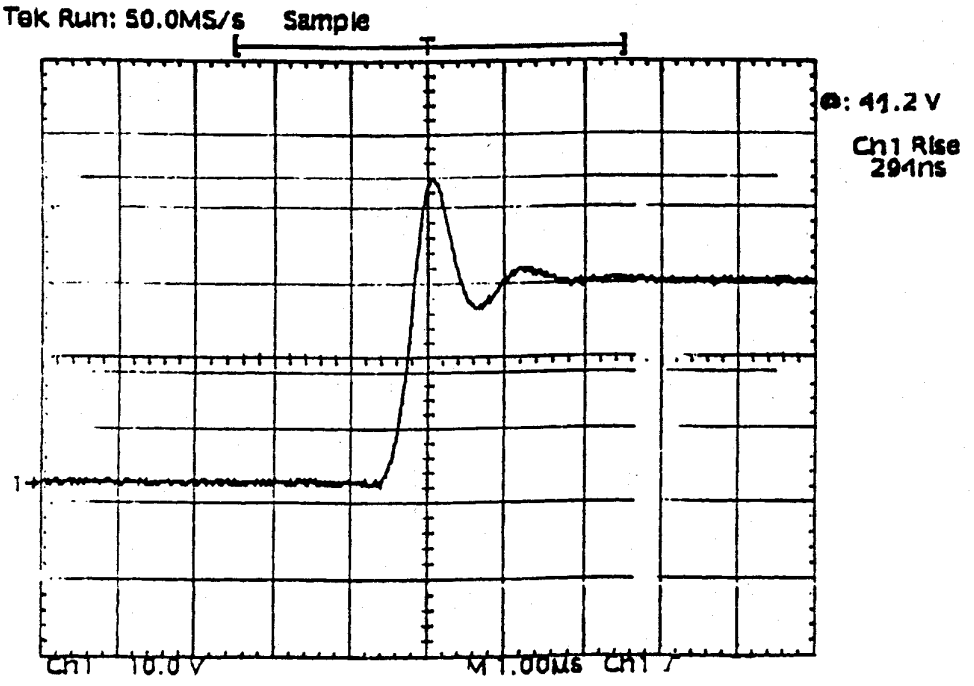

(a)

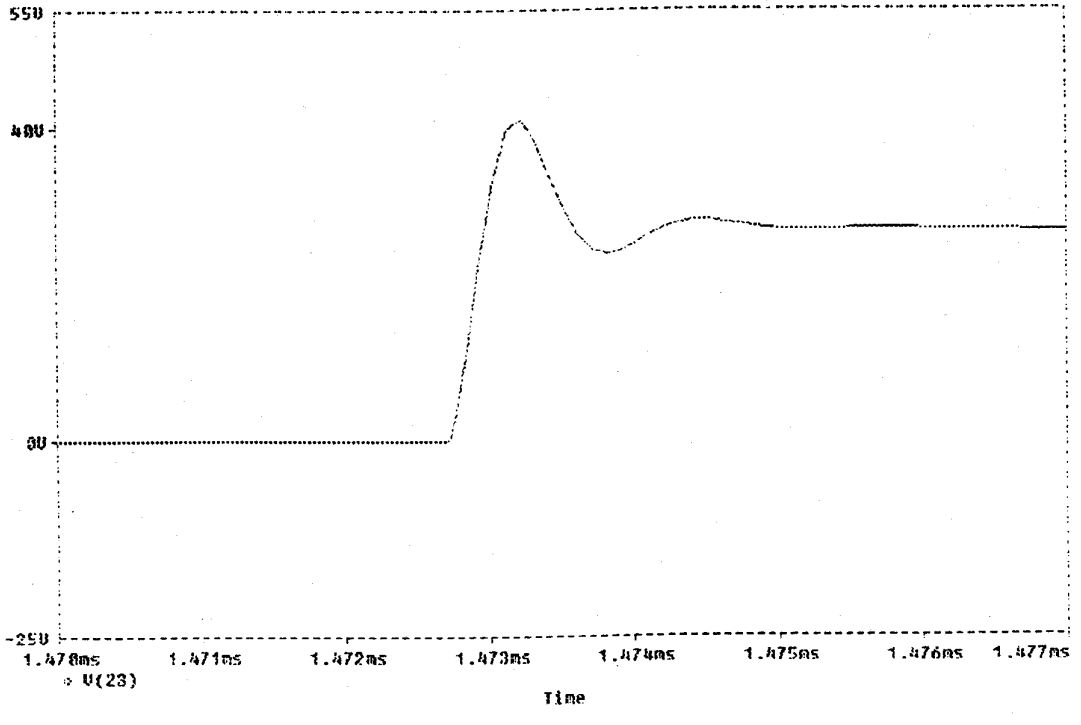

(b)

Fig. 7. Detailed view of the load voltage over-shoot: (a) measured and (b) computed.

given by the well-known expression for the electrostatic field of a point charge

$$E_{stm,n} = \frac{Q_{m,n}}{4\pi\varepsilon_0 r^3} x\boldsymbol{i} + \frac{Q_{m,n}}{4\pi\varepsilon_0 r^3} y\boldsymbol{j} + \frac{Q_{m,n}}{4\pi\varepsilon_0 r^3} z\boldsymbol{k} \qquad (9)$$

where r is the distance from the junction to P, x, y and z are the coordinates of P, with respect to the junction, and $\boldsymbol{i}, \boldsymbol{j}$ and $\boldsymbol{k}$ are the unit vectors along the axis.

Using (7)–(9) calls for a segmentation of the traces so that the dipole lengths are significantly smaller than the minimum

TABLE III
LOAD VOLTAGE

	Measured O.C.1	Computed O.C.1	Measured O.C.2	Computed O.C.2
V_{peak} [V]	30.8	30.8	41.15	41.2
Rise time [μs]	1.08	0.98	0.294	0.300
Fall time [μs]	0.130	0.140	0.120	0.130

TABLE IV
LOAD VOLTAGE

	Measured O.C.3	Computed O.C.3	Measured O.C.4	Computed O.C.4
V_{peak} [V]	36.6	36.6	21.8	21.8
Rise time [ns]	980	900	151	145
Fall time [ns]	120	130	125	110

wavelength associated with the transient and the distance to the observation point P. This is always more restrictive (more segments are needed) than the required segmentation for current evaluation, and for the frequency spectrum of an SMPS a subdivision into ten segments for each trace provides reasonable accuracy.

IV. MODEL VALIDATION

The converter section of the SMPS in Fig. 1 has the geometrical characteristics reported in Table I.

From these values the electrical parameters needed for the numerical simulation are evaluated and summarized in Table II.

A heuristic procedure has been adopted in order to insure that the number of lumped Pi sections of Fig. 2(b) is also able to describe possible resonances due to the presence of reactive elements: the traces were modeled using an increasing number of cells until the difference between the current and voltage values in two successive discretizations (between 0 and 100 MHz) was less than 0.1%. Fig. 4 shows the complete PSpice circuit adopted for the simulation. The used MOSFET model in the simulation is an IRF440 built-in model belonging to the Pspice MOSFET library.

In order to validate the proposed method, four different operating conditions *(O.C.1,2,3* and *4)* of the SMPS are considered.

These are characterized by the source voltage $V_{\rm DC}$, the switching frequency f_s, the duty-cycle δ, and the value of the load, chosen as being the most significant for such a device.

$$\underline{O.C.\ 1}:\ V_{\rm DC} = 13\ {\rm V},\quad f_s = 75\ {\rm kHz},\quad d = 0.5,\quad R_{\rm load} = 1.2\ {\rm k}\Omega.$$

The presence of a pure resistive load gives a proportional relationship between voltage and current at the load. Fig. 5 shows a comparison between measured and calculated load voltage. The small over-shoot at the right-hand edge of each pulse in the measured voltage [Fig. 5(a)] also occurs in the calculated one [Fig. 5(b)]. Table III compares the most significant transient magnitudes for such an operating condition.

$$\underline{O.C.\ 2}:\ V_{\rm DC} = 13\ {\rm V},\quad f_s = 75\ {\rm kHz},\quad d = 0.5,\quad R_{\rm load} = 470\ \Omega,\quad L_{\rm load} = 0.1\ {\rm mH}.$$

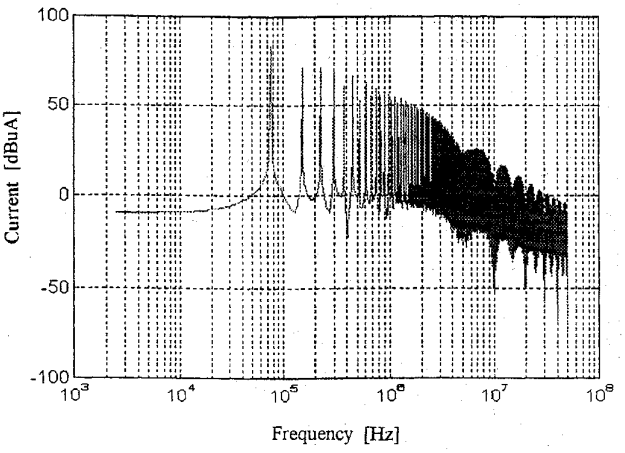

Fig. 8. Frequency spectrum of the load current for O.C. 1.

This set of operating parameters is particularly useful to test the prediction capabilities of the proposed approach. The peak value and the over-shoot of the measured load voltage [Fig. 6(a)] are fully predicted by the computed values in Fig. 6(b). Fig. 7 shows a detailed picture of the measured [Fig. 7(a)] and calculated [Fig. 7(b)] over-shoot and their agreement. Table III summarizes the results.

Two more conditions are considered: *O.C. 3* ($V_{\rm DC} = 13$ V, $f_s = 150$ kHz, $\delta = 0.5, R_{\rm load} = 1.2\,{\rm k}\Omega$) and *O.C.4* ($V_{\rm DC} = 13$ V, $f_s = 150$ kHz, $\delta = 0.3, R_{\rm load} = 1.2\,{\rm k}\Omega$). For the sake of brevity, only the recapitulatory Table IV is presented: it shows the reliability of the developed approach for evaluating the SMPS voltages and currents for different load values, f_s and δ, in order to predict the radiated electromagnetic field.

Computation of the EM near-field radiated by the converter section, for analysis of the EMI produced on the control section, is carried out in frequency domain. The time waveform of the current flowing on each segment into which the Pspice circuit is divided is Fourier transformed by an accurate FFT algorithm [9]. These currents are the sources of the radiated EM field, evaluated by means of the algorithm described in Section III. Fig. 8 shows the frequency spectrum of the load current for operating condition 1. The geometry of the radiating structure is given in Fig. 9 and the dimensions of the traces are those reported in Table I. The effects of omitting

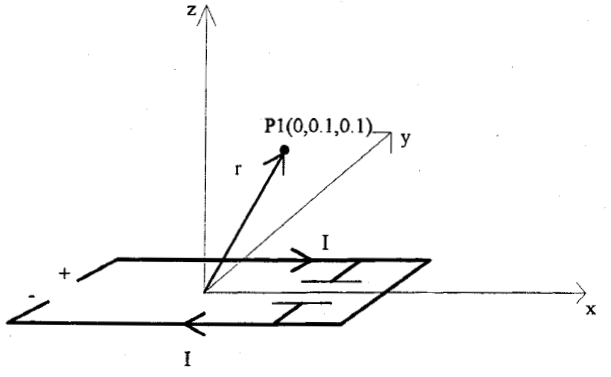

Fig. 9. Geometry of the radiating structure.

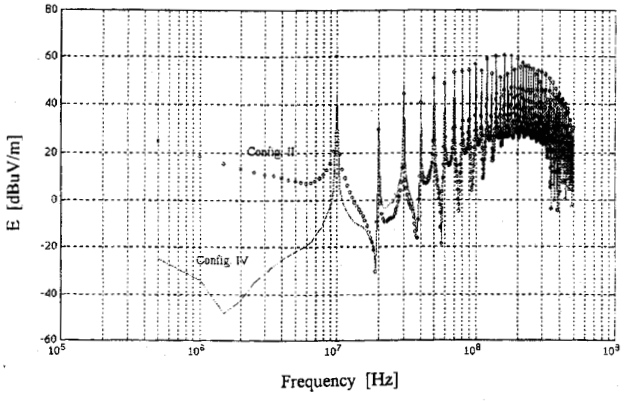

Fig. 10. $\boldsymbol{E}(\omega)$ in $P(0., 0., 3.)$: (o o o) classical approach, (- - -) modified dipole equations.

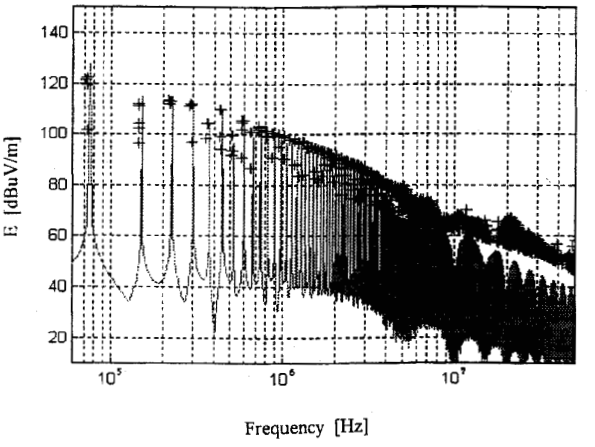

(a)

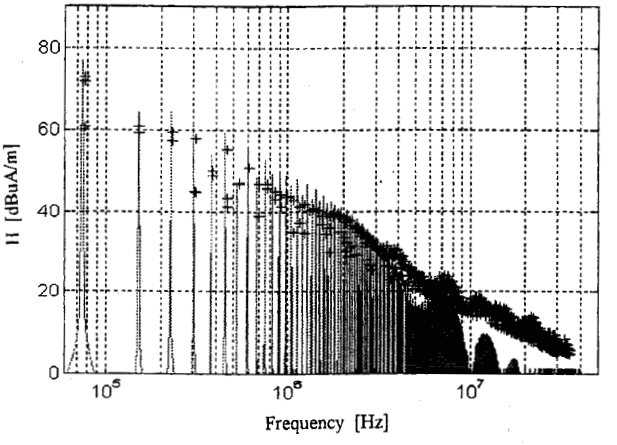

(b)

Fig. 11. (a) $\boldsymbol{E}(\omega)$ in $P_1(0., 0.1, 0.1)$: (+) measured, (- - -) computed. (b) $\boldsymbol{H}(\omega)$ in $P(0., 0.1, 0.1)$: (+) measured, (- - -) computed.

the fictitious electrostatic terms in the dipole equations, as described in Section III, are evident from Fig. 10, where the radiated electric field at $P(0.$ m, $0.$ m, $3.$ m) derived by the classical equations (circles) is compared with that stemming from the modified one. A difference of about 40 dB appears at low frequencies, where the electrostatic terms in (7) are dominant. As the frequency increases, the results from these two approaches tend to coincide and above 15 MHz , as expected, they overlap perfectly. To test the validity of the proposed radiation model two points P_1 (0. m, 0.1 m, 0.1 m) and P_2 (0. m, 0. m, 0.1 m) very close to the SMPS converter section have been chosen for calculation of the EM fields. Figs. 11(a) and 12(a) show the comparison between the measured and calculated values of the electric field, while the magnetic fields are compared in Figs. 11(b) and 12(b). In both cases, the agreement between measured and computed values is excellent up to 10 MHz. Above this frequency the presence of the common mode currents can no longer be neglected and the TL model of the circuit does not give a correct estimation of the currents and, hence, of the fields. In any case, as shown by Figs. 8 and 11, the energy content of currents and fields due to an SMPS is limited in the low-frequency region below 1–5 MHz, where the effects of the differential mode current are dominant.

From this approach one can obtain useful data such as far-field radiation patterns [12], near-field maps, and electromagnetic energy distributions [13] for the correct EMC design of the device.

V. Conclusions

The proposed analysis permits some conclusions to be drawn concerning the EMC modeling of SMPS. Because the switching frequencies of such devices are no more than a few hundred kilohertz, the energy content of the harmonic components currents, voltages, and radiated fields is limited below 10–15 MHz. The radiation from the SMPS's converter section is not of serious concern for compliance with EMC Standards, but it is for the correct operation of the control section, which is usually placed very close by. In this frequency range the whole circuit is well modeled as a TL in which the conductors lie between two media with different permittivity. The introduction of a suitable equivalent permittivity allows extension of the TL theory for homogeneous medium to this case. There is excellent agreement between measured and computed results for different operating conditions of the SMPS. As the frequency increases, the common mode currents become important, due to parasitic couplings, and the TL

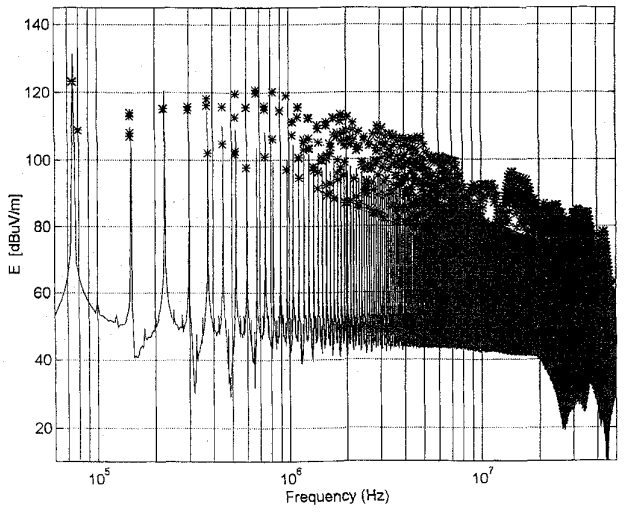

(a)

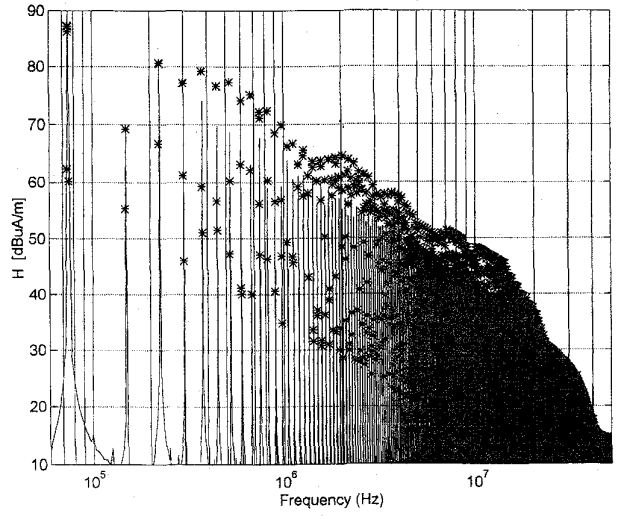

(b)

Fig. 12. (a) $\boldsymbol{E}(\omega)$ in $P_2(0., 0., 0.1)$: (+) measured, (---) computed. (b) $\boldsymbol{H}(\omega)$ in $P(0., 0., 0.1)$: (+) measured, (---) computed.

model fails to represent correctly the current distribution along the circuit. In the near-field calculations the radiating structure of the SMPS is divided into a suitable number of finite length electric dipoles. An adequate treatment of the dipole equations is needed: the field of a fictitious electrostatic charge at the junction between two equal dipoles carrying the same current, due to the finite length segmentation, must be subtracted from the total field in order to get an exact evaluation of the radiated em field. In this case, too, the measurements performed confirm the validity of such a procedure.

APPENDIX A

In terms of Jacobian elliptic functions, the modulus k and the complementary modulus k' are related with the parameter m_1 by

$$k^2 = m, \quad k'^2 = m_1 \tag{A1}$$

$$m + m_1 = 1. \tag{A2}$$

The complete elliptic integral of the first kind (5a) and its complementary integral in terms of m_1 are

$$K = K(m) = \int_0^1 \frac{dt}{[(1-t^2)(1-mt^2)]^{1/2}} \tag{A3}$$

$$K' = K(m_1) = K(1-m). \tag{A4}$$

Equations (A3) and (A4) can be expressed in terms of infinite series [14] and their ratio is

$$K/K' = -\pi/\ln q \tag{A5}$$

where

$$q = m/16 + 8(m/16)^2 + 84(m/16)^3 + 992(m/16)^4 + \cdots. \tag{A6}$$

Substituting k and k' to m and m_1 in (A6) and using the first three terms gives

$$\frac{K(k)}{K'(k)} = \begin{cases} \pi \Big/ \left[0.69 + \ln \dfrac{1+(1-k^2)^{1/4}}{1-(1-k^2)^{1/4}}\right] \\ \qquad \text{for } 0 < k < 0.707 \end{cases} \tag{A7a}$$

$$\begin{cases} 0.22 + \dfrac{1}{\pi} \ln \dfrac{1+k^{1/2}}{1-k^{1/2}} \\ \qquad \text{for } 0.707 < k < 1 \end{cases} \tag{A7b}$$

These expressions are equivalent to that presented in [15] and are easier to calculate.

REFERENCES

[1] IEC Draft 22G-WG4-11 "Electromagnetic compatibility of power drive systems," Oct. 1994.
[2] J. Roudet, R. Scheich, and V. Handel, "EMI conducted emission in differential mode emanating from a SCR: Phenomena and noise level prediction," in *Proc. IEEE 1993 APEC*, San Diego, CA, 1993.
[3] J. Roudet, R. Scheich, and A. Orlandi, "Origin and propagation of common mode currents occurring in a bridge rectifier," in *Proc. 15th Int. Telecommun. Energy Conf.* Paris, France, Sept. 27–30, 1993.
[4] J. Roudet, R. Scheich, and J. Mahdavi, "Conducted RFI emission from AC/DC converter with sinusoidal line current," in *Proc. IEEE 1993 IAS Conf.*, Toronto, Canada, 1993.
[5] G. Antonini, "Caratterizzazione elettromagnetica di dispositivi SMPS: modello e verifica sperimentale delle emissioni radiate" (in Italian), *Laurea Thesis*, University of L'Aquila, Italy, July 1994.
[6] D. W. P. Thomas, C. Cristopulos, and E.T.Pereira, "Calculation of radiated electromagnetic fields from cables ussing time-domain simulation," *IEEE Trans. Electromag. Compat.*, vol. 36, Aug. 1994.
[7] H. A. Wheeler, "Transmission line properties of parallel strips separated by a dielectric sheet," *IEEE Trans. Microwave Theory Tech.*, MTT-13, 172–185, 1965.
[8] T. C. Edwards, *Foundations for Microstrip Engineering*. New York: Wiley, 1981.
[9] M. Rashid, *SPICE for Circuits and Electronics Using PSpice*. Englewood Cliffs, NJ: Prentice-Hall, 1990.
[10] S. Ramo, J. R. Whinnery, and T. Van Duzer, *Fields and Waves in Communication Electronics*. New York: Wiley, 1994.
[11] W. H. Press, B. P. Flannery, S. A. Teukolsky, and W. T. Vetterling, *Numerical Recipes: The Art of Scientific Computing*. New York: Cambridge University Press, 1989.
[12] A. Orlandi and R. Scheich, "EMC in power electronic devices: Radiated emissions from a silicon controlled rectifier," in *Proc. IEEE Int. Symp. Electromag. Compat.*, Chicago, IL, Aug. 22–27, 1994.
[13] F. Antonini, S. Cristina, and A. Orlandi, "Switched mode power supplies EMC analysis: Near-field modeling and experimental validation," in *Proc. IEEE Int. Symp. Electromag. Compat.*, Atlanta, GA, Aug. 14–18, 1995.
[14] M. Abramowitz and I. Stegun, *Handbook of Mathematical Functions*. New York: Dover Publications, 1972.
[15] K. C. Gupta, R. Garg, and I. J. Bahl, *Microstrip Lines and Slotlines*. Dedham, MA: Artech House, 1981.

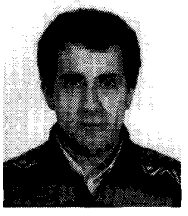

Giulio Antonini was born in Avezzano, Italy, in January 1969. He received the Laurea degree in electrical engineering in 1994 from the University of L'Aquila. He is currently working toward the Ph.D. degree in electrical engineering at the University of Rome "La Sapienza," Italy.

His research interests are shields models and EMI analysis from power drives systems.

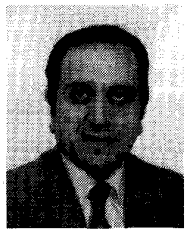

Saverio Cristina (M'76–SM'83) was born in Montevago, Italy, on October 18, 1948. He received the degree in electrical engineering from the University of Rome, Italy, in 1974.

Since then, he has been working at the University's Department of Electrical Engineering. He was a Researcher until 1978, an Assistant Professor from 1978 to 1982, and an Associate Professor from 1982 to 1986. At present, he is a Full Professor of basic electrical engineering at the University of L'Aquilla, Italy. He has published a number of papers in the fields of corona, wave propagation, power system communications, electromagnetic compatibility, and numerical computation of electromagnetic fields. His current research interests include the numerical computation of ionized electric fields in electrostatic precipitators and electromagnetic compatibility.

Mr. Cristina is a Member of CIGRE and of the IEEE/PES Corona and Field Effects Subcommittee.

Antonio Orlandi (M'90) was born in Milan, Italy, on September 16, 1963. He received the degree in electrical engineering in 1988 from the University of Rome, Italy.

From 1988 to 1990, he was with the Department of Electrical Engineering at the University of Rome. In 1990, he was appointed Assistant Professor of the Electrical Engineering Department at the University of L'Aquila, Italy. He has published papers in the fields of electromagnetic compatibility and lightning protection systems. Current research interests include numerical method to approach EMC problems, EMI from HV substations and ac–dc power converters, and very fast transients characterization techniques.

Dr. Orlandi is an Associate Editor of the IEEE TRANSACTIONS ON ELECTROMAGNETIC COMPATIBILITY and a member of the IEEE EMCS TC-9 Committee.